JACS
JOURNAL OF THE AMERICAN CHEMICAL SOCIETY

Article

pubs.acs.org/JACS

Healable Supramolecular Polymers as Organic Metals

Joseph J. Armao, IV,[†] Mounir Maaloum,[†] Thomas Ellis,[†] Gad Fuks,[†] Michel Rawiso,[†] Emilie Moulin,[†] and Nicolas Giuseppone*,[†]

[†]SAMS research group, University of Strasbourg, Institut Charles Sadron, CNRS, 23 rue du Loess, BP 84047, 67034 Strasbourg Cedex 2, France

Supporting Information

ABSTRACT: Organic materials exhibiting metallic behavior are promising for numerous applications ranging from printed nanocircuits to large area electronics. However, the optimization of electronic conduction in organic metals such as charge-transfer salts or doped conjugated polymers requires high crystallinity, which is detrimental to their processability. To overcome this problem, the combination of the electronic properties of metal-like materials with the mechanical properties of soft self-assembled systems is attractive but necessitates the absence of structural defects in a regular lattice. Here we describe a one-dimensional supramolecular polymer in which photoinduced through-space charge-transfer complexes lead to highly coherent domains with delocalized electronic states displaying metallic behavior. We also reveal that diffusion of supramolecular polarons in the nanowires repairs structural defects thereby improving their conduction. The ability to access metallic properties from mendable self-assemblies extends the current understanding of both fields and opens a wide range of processing techniques for applications in organic electronics.

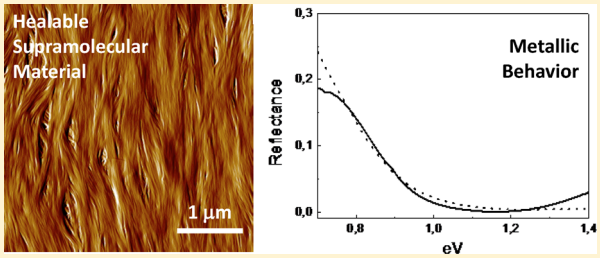

INTRODUCTION

One of the current challenges facing information technologies is the development of lightweight, low cost, and disposable plastic or paper electronic devices.[1,2] Conventional inorganic semiconductors (e.g., silicon) and conductors (e.g., metals) are expensive and rigid and commonly require multiple etching and lithographic steps for device fabrication. The discovery of chemically or electrochemically doped conjugated polymers and their implementation in organic electronics has been instrumental to overcome some of these problems.[3,4] Many soluble and processable semiconducting conjugated and supramolecular polymers have been synthesized and incorporated as active layers in devices such as OFETs (organic field effect transistors),[5] OLEDs (organic light emitting diodes),[6] and OPVs (organic photovoltaics).[7] However, metallic organic polymers sharing the electrical, electronic, magnetic, and optical properties of metals[8] are still very scarce although very promising for the development of a number of technologies such as transparent electrodes,[9,10] printed electronic circuits and interconnects,[11,12] thermoelectric materials,[13,14] or memory devices.[15] To reach such properties, oxidative or reductive doping should produce unpaired electrons that open a partially filled conduction band where charge carriers drift with minimal scattering as is the case in metals.[16] Defects enormously affect such conductivity, resulting in localized electronic states which alter the transport mechanism from band-like to undesired thermally activated hopping.[17,18] As a result, after four decades of materials developments, only a few number of organic structures have reached the landmark of metallic conductivity.[19] For conjugated polymers, chain-ordered polyaniline with a low density of structural defects was recently obtained by dispersion synthesis, showing a dramatic transition from an insulating to a metallic material upon doping, and with an increase in conductivity over 9 orders of magnitude.[20] Still, the poor solubility of doped polyaniline limits its use for a number of processing techniques. Another kind of organic metal is based on charge transfer complexes such as TTF-TCNQ salts,[21] which are single-crystals and lack the processability and mechanical properties required by flexible electronic devices. In a third example, our group has recently shown that chemically tailored triarylamine molecules can be grown in the form of one-dimensional supramolecular polymers[22] directly between electrodes at the 100 nm length scale.[23] These nanowires showed increasing conductivity with decreasing temperature down to 1.5 K, both in the bulk and at interface with electrodes (with values $>5 \times 10^3$ S m^{-1}). However, the crystalline nature of the fibers originating from a kinetically controlled nucleation/growth process traps structural defects in the π-stacking structure over larger length scales, and disconnections of the rigid nanorods produce grain boundaries which are detrimental for conductivity.

We herein describe a new class of conducting but very soft and kinetically labile supramolecular triarylamines,[24] i.e., in which reorganization of the molecular units can take place with a relatively low activation energy. In such a configuration, the reversible nature of the supramolecular interactions can in principle correct structural defects (i.e., lateral or rotational

Received: May 7, 2014
Published: July 23, 2014

ACS Publications © 2014 American Chemical Society

dx.doi.org/10.1021/ja5044006 | J. Am. Chem. Soc. 2014, 136, 11382−11388

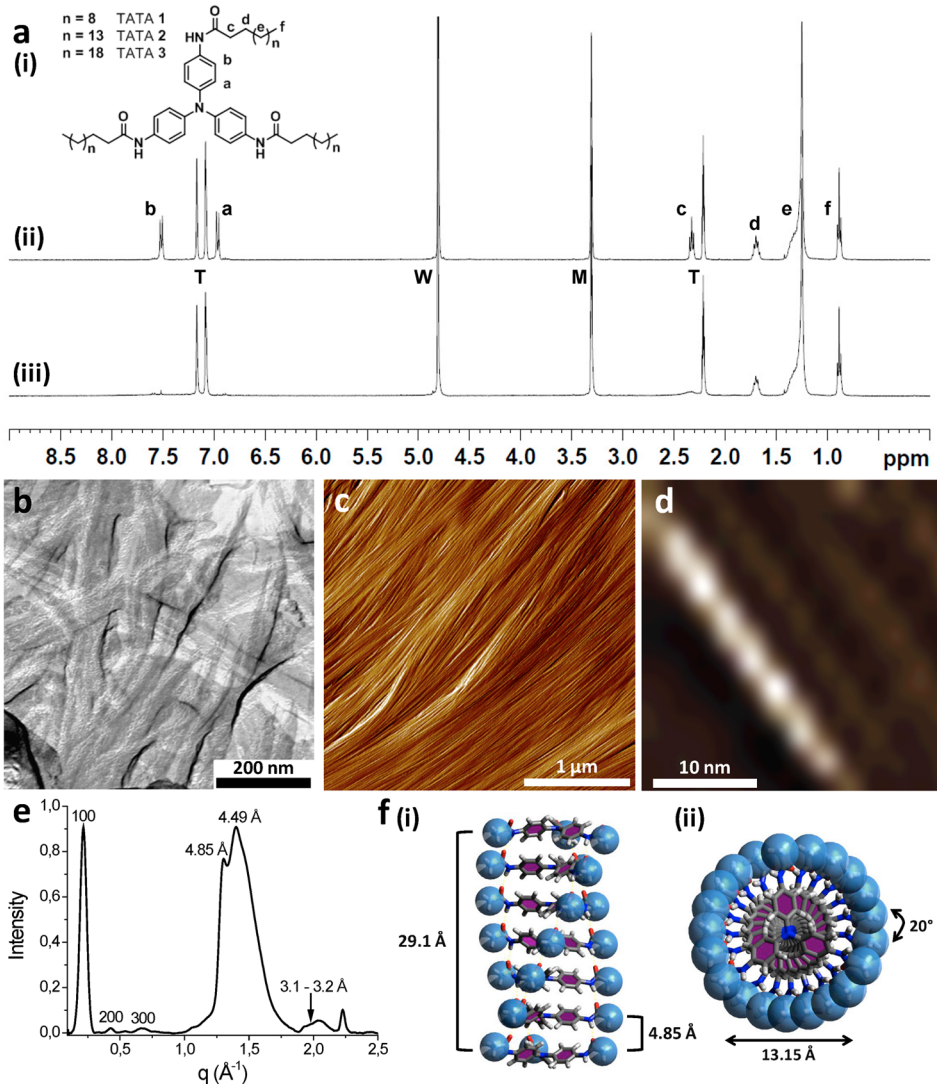

Figure 1. Structural characteristics of TATA self-assemblies. (a) (i) Chemical formula of TATA **1**, **2**, **3** and associated ^{1}H NMR of TATA **1** in a 5:3 methanol-d_4:toluene-d_8 mixture, in the presence of $CDCl_3$ (5 vol %) before (ii) and after (iii) light irradiation (W, M, and T are the residual resonance peaks for water, methanol, and toluene, respectively). (b) Freeze-fracture TEM image of TATA **1** showing its native form in chloroform. (c,d) AFM imaging of TATA **1** at the micrometer scale (c) and at the nanometer scale for a single fiber (d) obtained from a chloroform solution drop cast on mica. (e) X-ray scattering of a thin film of TATA **1** prepared from a drop cast film on mica. (f) Side view (i) and top view (ii) of the proposed stacking structure of TATA **1**, as obtained from DFT calculations, and with a longitudinal periodicity of 29.1 Å, a nitrogen−nitrogen distance of 4.85 Å between adjacent molecules, and a dihedral angle of 20° between each plateau.

misalignments of the stacks) by reaching a lower energetic state under thermodynamic control (self-healing polymers).[25,26] We show that a proper balance between order and mobility leads to materials presenting a unique combination of functionalities, namely extended metallic character with soft mechanical and defect-healing properties.

RESULTS AND DISCUSSION

The original molecular units of this study, namely tris-amide triarylamines with various alkyl side chains (TATA **1**−**3**, Figure 1a(i)), were obtained with good yields in a three step process (see the Supporting Information for the synthetic procedures). At a concentration of 5 mM in a deuterated 5:3 methanol:toluene mixture, **1** is soluble and a full NMR spectrum can be recorded (Figure 1a(ii)). Interestingly, upon the addition of deuterated chloroform (5 vol %) as an electron acceptor, it is possible to trigger a self-assembly process by a pulse of white light which oxidizes a catalytic quantity of TATA to its radical cation TATA$^{\cdot+}$. Aggregation of these radicals at a critical nucleation concentration promotes the stacking of neutral TATA molecules in a subsequent growth process.[22] The clear signature of this self-assembly is the disappearance of the **a**, **b**, and **c** resonance signals due to a strong π-stacking between TATA cores and resulting in an anisotropic columnar system kept soluble by lateral flexible alkyl chains (Figure 1a(iii)). In a variety of pure organic solvents (chloroform, acetonitrile, acetone, or toluene), ^{1}H NMR reveals the direct self-assembly of TATA **1**−**3** without the need of light. Intermolecular hydrogen bonding also participates in the self-assembly as observed by infrared spectroscopy, which displays the characteristic shifts of the amide stretching frequencies with the N−H and C═O stretching vibration occurring at 3291 and 1654 cm^{-1}, respectively.[27] At the macroscopic level and above a critical concentration, **1** forms a soft physical gel in chloroform with a melting enthalpy of 7.6 KJ mol^{-1} at 35.7 °C. Differential scanning calorimetry (DSC) also reveals a decreasing critical

dx.doi.org/10.1021/ja5044006 | J. Am. Chem. Soc. 2014, 136, 11382−11388

gelation concentration and an increasing melting enthalpy for longer alkyl chains (TATA **2** and **3**; Figure S1 and Table S1). Insight in the structure of this self-assembly is first given by freeze fracture transmission electron microscopy (FFTEM) in the gel state (Figure 1b), and by atomic force microscopy (AFM) of cast films obtained from dilute chloroform solutions (Figure 1c and Figure S2). Well-defined fibers of more than ten micrometers long and of high persistence length are characteristic of such compounds. For TATA **1**, high resolution AFM shows a diameter of 16(±3.0) Å for the individual fibers (Figure 1d and Figure S2), which also present a twisted periodic pattern of 30.0(±2.0) Å along their main axis. A model of the molecular assembly was built up using complementary small angle and wide-angle X-ray scattering (SAXS and WAXS; Figure 1e), together with density functional theory (DFT; Figure 1f).[28−30] Strong 100 scattering peak at 0.215 $Å^{-1}$ as well as weaker 200 and 300 reflections are characteristic of a smectic-type packing with a periodicity of 29.1 Å along the one-dimensional ordering of the molecules (similar to the periodicity observed by AFM, Figure 2b). The large peak at 1.30 $Å^{-1}$ corresponds to a distance of 4.85 Å between nitrogen centers of adjacent triarylamines, in agreement with DFT results. The apparent pitch (which is due to the 3-fold symmetry of the TATA core), together with the stacking distance, imply that 7 molecules are contained in a single period with a dihedral angle of 20° between them, a value also in agreement with DFT calculations. The broad scattering peak centered at 1.40 $Å^{-1}$ corresponds to amorphous packing of the alkyl chains, and the small peak around 2 $Å^{-1}$ corresponds to an aryl $\pi-\pi$ stacking distance of 3.1−3.2 Å. DFT predicts a similar stacking distance due to both the tilt of the aromatic rings and the dihedral angle between the molecules.

Exposure of preassembled TATA fibers to visible light in chloroform leads to the appearance of an absorption band in the near-infrared (NIR), with a complex behavior as a function of irradiation time (Figure 2a,b). Similar bands have been described in the literature for mixed valence charge transfer between bis-triarylamine molecules linked by conjugated covalent bonds.[31] Interestingly, in our system, the presence of such a characteristic absorption band (λ_{max} = 1100 nm) can only arise from an intermolecular through-space charge-transfer between stacked triarylamine cores. In the literature, mixed-valence charge transfers have been classified depending on the nature of the electronic delocalization between the redox centers.[32] Class I systems consist of localized redox centers, while class II are partially delocalized, and class III fully delocalized. The shape of the charge transfer band can give insight into the nature of the interaction, with a Gaussian shaped band expected for a class II charge transfer and an asymmetric band expected for a class III (see the Supporting Information). Here, increasing asymmetry observed between 0 and 30 min of irradiation (Figure S16a) indicates an increasing contribution from fully delocalized class III charge transfers. The absorption band at 800 nm, starting at 5 min and increasing in intensity for the remainder of the irradiation experiment, corresponds to a higher contribution of localized class I triarylamine cation.

Electronic paramagnetic resonance spectroscopy (EPR) provides both a quantification of the amount of radicals within the fibers as well as an alternative means of investigating the nature of the charge transfer relative to the EPR time scale. The hyperfine splitting of the EPR signal, arising from a through-space hyperfine coupling of adjacent triarylamine nitrogen

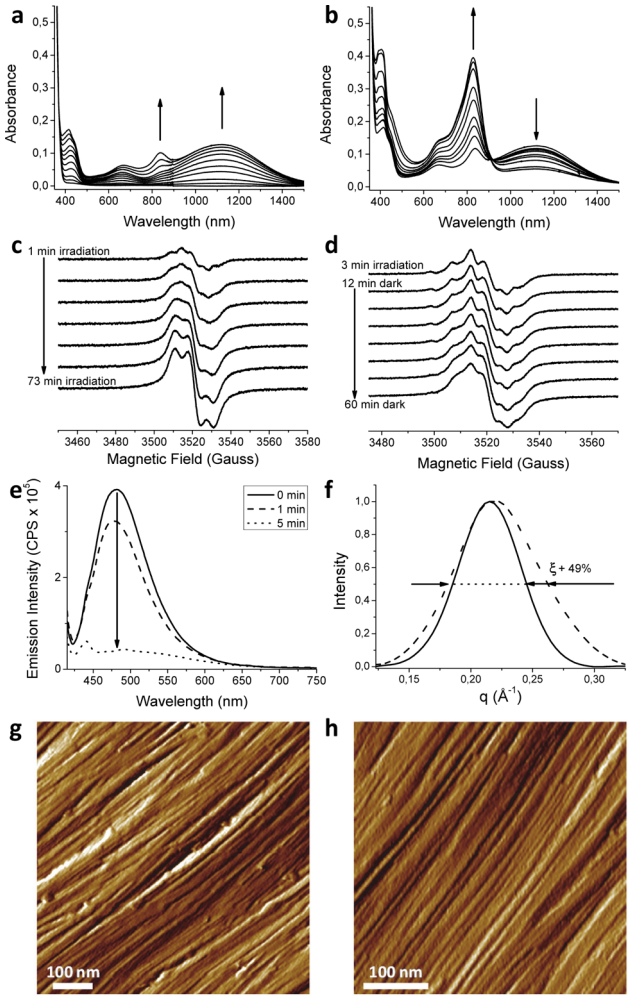

Figure 2. Effect of light irradiation on TATA self-assemblies. (a,b) Sequential absorbance spectra taken during light irradiation (with a halogen lamp; 10 W cm^{-2}) of a 0.1 mM solution of TATA **1** in $CHCl_3$; (a) first 6 min of light irradiation, (b) from 7 to 73 min of light irradiation. (c) Room temperature EPR spectra taken while irradiating (with a halogen lamp; 10 W cm^{-2}) a 1 mM solution of TATA **1** in $CHCl_3$ from 1 to 73 min. (d) Room temperature EPR spectra taken for a sample irradiated for 3 minutes, and subsequently put in the dark for 60 min. (e) Fluorescence emission of TATA **1** upon light irradiation showing the quenching induced by the polaron formation. (f) SAXS of nonirradiated (dotted line) and irradiated (full line) thin films demonstrating a 49% increase in the correlation length (calculated as 4π/fwhm). (g−h) AFM image of TATA 1 obtained from the drop cast of a chloroform solution before light irradiation (g) and after 15 min of light irradiation (h) showing the healing of structural defects. In (f) and (g) the nonirradiated solutions were kept 15 min in the dark to discriminate the effect of light from a possible aging effect.

centers, displays an evolution with the time of light irradiation (Figure 2c and Figures S16b and S17a). Three distinct although partially overlapped periods are observed with (i) the growth of a smooth five line signal corresponding to irradiation times from 15 s to 7 min (0−15 mol % of radicals); (ii) an evolution toward a one line pattern from 7 to 18 min (15−25 mol % of radicals), and (iii) the emergence of a 3-line pattern from 23 to 73 min (29−44 mol % of radicals). In the literature, EPR studies of covalently linked mixed-valence bis-triarylamines show similar splitting patterns.[33] By analogy, the five line pattern corresponds to partially delocalized unpaired electrons

dx.doi.org/10.1021/ja5044006 | J. Am. Chem. Soc. 2014, 136, 11382−11388

between two triarylamines; the one line pattern, to a fully delocalized system with no energetic barrier to charge transfer; and the three line pattern, to unpaired electrons which are localized on one triarylamine.

Thus, both EPR and NIR data demonstrate the initial formation of a mixed population of classes II and III charge transfers, followed by a transition to a single population of class III, which then tends to a localized class I as the higher number of charges in the one-dimensional fiber leads to electrostatic repulsion. A complementary experiment was performed by irradiating a solution for 3 min and by then following the evolution of the radicals in the dark (Figure 2d). Interestingly, the change of the EPR signal toward a one-line pattern was observed over 1 h. This indicates that the transformation from class II to class III charge transfers is not related to the number of radicals, and suggests an intrinsic structural evolution of the system with time.

To understand the relationship between the nature of the charge transfer and the irradiation time, we compared the X-ray scattering profiles of two thin films; one made from a nonirradiated solution, and the other one from a solution irradiated for 15 min (Figure 2f). A Gaussian fit of the peak at 0.215 $Å^{-1}$ revealed a noticeable decrease in the peak width at half-maximum, demonstrating an increase of the fiber correlation length (ξ) of 49%, going from 163 Å in the dark to 243 Å upon irradiation (Figure S6). The 300 reflection of the irradiated sample also displays a noticeable sharpening, indicating a decreasing cumulative disorder, i.e. a fewer number of structural defects with light.[34] Characterization of numerous samples using high resolution AFM unambiguously confirmed the improved ordering of the fibers, as well as the self-healing of the gel in the 100 nm range, upon light irradiation (Figure 2g,h and Figures S4 and S5). Altogether, these results strongly suggest that class III charge transfer occurs between molecules in a thermodynamic minimum while class II charge transfer occurs at small structural defects in the self-assembly where the electronic coupling and reorganization energy are less efficient. DFT calculations also support a class III delocalized charge transfer in the optimized assembly geometry within the framework of Marcus–Hush theory (Figure 3a–c and Figures S10–S12).[35,36]

We propose to describe this type of charge transfer complex migrating through the fibers as a "supramolecular polaron", which consists in a "through-space" version of the polarons observed in conjugated polymers, and associating the radical cation with a lattice deformation.[16] This is also in agreement with further fluorescence experiments which show exciton quenching by the supramolecular polarons as is commonly observed with polarons in conjugated polymers (Figure 2e and the Supporting Information).[37,38] For TATA **1**, DFT calculations give an optimized binding energy of 16.2 kcal/mol for the neutral dimer and of 37.1 kcal/mol for the radical cation dimer, demonstrating a sufficient energetic gain to heal defects (i.e., lateral or rotational misalignements) in the course of their diffusion through the columnar stacks.

In the presence of these polarons, the supramolecular polymer presents unique and clear signatures of metallic behavior. For instance, temperature-dependent EPR measurements were performed down to 4 K on the powder obtained from irradiated fibers, and a plot of the inverse EPR signal versus temperature displays two distinct regions (Figure 4a). The lower temperature region below 90 K shows a linear dependence, indicating that the signal is arising from unpaired

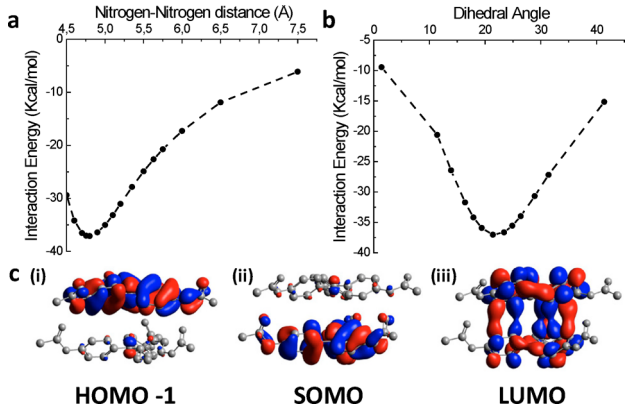

Figure 3. DFT optimized geometry for TATA self-assemblies. (a,b) Interactions energies determined by DFT for a generic (i.e., with a single lateral methyl group instead of the alkyl chain) monocationic dimer of TATA as a function of the Nitrogen–Nitrogen distance (a) and the dihedral angle (b). (c) (i) HOMO, (ii) SOMO, and (iii) LUMO orbitals of a generic TATA monocationic dimer, as determined by DFT calculations in the optimized geometry.

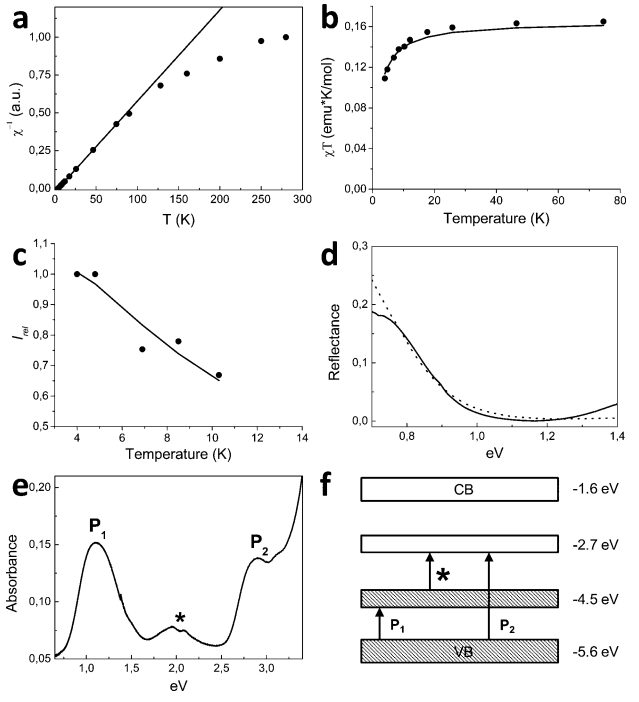

Figure 4. Metallic characteristics of TATA self-assemblies. (a) Temperature-dependent EPR measurement of TATA **1** displaying a low-temperature region consisting entirely of localized Curie spins (see linear behavior) and a higher temperature region displaying a mixture of Curie and delocalized Pauli spins. (b) Fit of χT vs T with the Curie–Weiss law for data between 4 and 80 K (r^2 = 0.999). (c) Relative intensity of the half-field EPR transition versus temperature. The data were fitted with the Bleaney–Bowers model giving a weak antiferromagnetic coupling with J = −0.48 K (r^2 = 0.998). (d) Reflectance measurements of an irradiated thin film of TATA **1** displaying a plasma resonance near 1.2 eV, typical of delocalized metallic electrons and theoretical fit of the reflectance with the Drude model (dotted line), $\varepsilon(\omega) = \varepsilon^{\infty} - \omega_p^2\tau^2(1 + \omega^2\tau^2)^{-1}$. (e) Absorption spectrum of an irradiated thin film of TATA **1** displaying optical signatures of polaronic bands. (f) Determined band structure calculated from absorbance measurements in (e) and showing a half-filled polaronic band at −4.5 eV.

dx.doi.org/10.1021/ja5044006 | J. Am. Chem. Soc. 2014, 136, 11382–11388

Curie spins within the fibers. Then, starting at 90 K and above, a deviation from Curie behavior indicates a contribution from Pauli spins, which should display temperature independent behavior and which are commonly observed in materials containing metallic electrons. In particular, a similar transition between low temperature Curie behavior and higher temperature Pauli or mixed Curie and Pauli behavior has been observed in films of metallic polyaniline.[39] Additionally, by fitting the curve in the low temperature region using the Curie−Weiss law, a value of −1.81 K was found for the Weiss constant which indicates a weak antiferromagnetic interaction between radicals within the fibers (Figure 4b). The weak half-field signal ($g \approx 4$), observed around 10 K and below, demonstrates exchange-coupling of the doublet electrons giving rise to singlet ($S = 0$) and triplet ($S = 1$) states. The half-field signal dependence with temperature was fitted with Bleaney−Bowers model[40] to give a value of $J = -0.48$ K (Figure 4c), which is also indicative of weak antiferromagnetic exchange-coupling and of a singlet ground state within the fibers. Following the method of Eaton, a distance of 3.73 Å was calculated between coupled spins at cryogenic temperatures indicating most of the spin density is on the aromatic carbons, in line with our DFT calculations.[41] Finally, a further signature of the metallic behavior comes from the reflectance measurements displaying a minimum around 1.2 eV. These data are well-fitted by the Drude model for a true metallic behavior which gives the values of the plasma frequency ($\omega_p = 1.16$ eV) and of the relaxation time ($\tau = 1.16 \times 10^{-14}$ s; Figure 4d).[20,42] In an irradiated thin film, and by using both EPR (Figure S17c) and absorption spectroscopy (Figure 4e), we observed a high stability of the radical which remains unchanged for at least six months. It is striking to observe a classic polaronic absorption signature as described for conducting conjugated polymers[43] and, from the two main absorptions, a polaronic conduction band with a half-filled energy level located at 1.1 eV above the valence band (Figure 4f).

In order to probe the effect of light on the fibers' conduction properties directly in a device, we have then used transparent ITO electrodes separated by a 4 μm gap. Conductivity measurements were performed with a dc current on fibers made of TATA **1**, **2**, and **3** (all at a concentration of 17 mM in tetrachloroethane), and on a nonself-assembling tri(bromophenyl)amine for control experiments (Figure 5a). Compared to this control, previous to light irradiation and under a 0.1 V bias (which is far below the oxidation potential of the triarylamine derivatives), conductivities of 2 orders of magnitude higher for **3**, and 4 orders of magnitude higher for **1** and **2** are observed, demonstrating conduction through the preformed fibers. Upon subsequent irradiation for 50 s, an increase of 2 orders of magnitude in conductivity is observed for TATA **1** and **2**, while the gel of **3** exhibits nearly a four-orders-of-magnitude increase, leading to a similar conductivity for the three TATAs after irradiation. This observation can be correlated to a larger fluorescence quenching in the case of TATA **3** (Figure S18). The measured conductivity then remains very stable in the dark, 6 orders of magnitude higher than the control molecule. We here consider that the contribution of ionic current is negligible because, in addition to its stability in the dark under a dc field and to the negligible response of the control molecule, the measured electronic conductivity remains unchanged when adding 10% of tetrabutylammonium chloride to the gel of **1**. It was also possible to affect the conductivity of the organogel without light

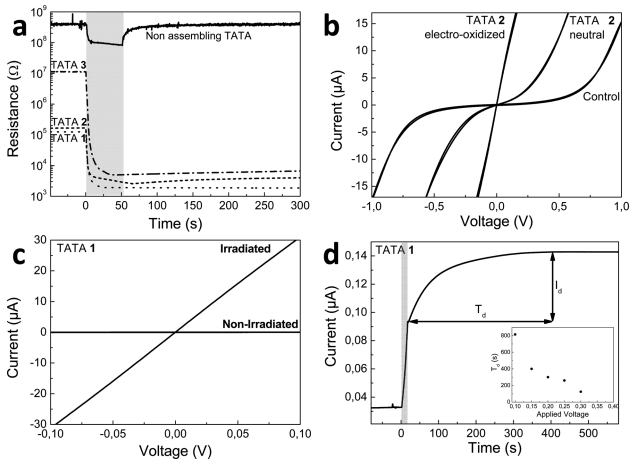

Figure 5. Combined influences of polarons' formation and diffusion on the conductivity of TATA self-assemblies. (a) Resistance versus time for 17 mM TATA samples in tetrachloroethane, and for a nonassembling tri(bromophenyl)amine as a control molecule. The gray background corresponds to the light irradiation time (halogen lamp; 10 W cm^{-2}). (b) $I-V$ curves for samples subjected to electrochemical oxidation. The control tri(bromophenyl)amine was subjected to an $I-V$ scan up to 2 V to ensure electrochemical oxidation. (c) $I-V$ curves before and after light-induced fibers formation of TATA **1** in a mixed solvent system of 5:3 methanol:toluene +5 vol % tetrachloroethane. (d) Dark conductivity increase time (T_d) after 15 s irradiation of TATA **1** (halogen lamp; 10 W cm^{-2}); the gray background corresponds to the light irradiation time. Inset displays the dependence of T_d on the applied voltage (see Figure S19 for the corresponding plots).

irradiation but, instead, by applying a difference of electric potential comprised between 0.6 and 0.8 V (that is crossing the oxidation potential of TATA). The $I-V$ curves demonstrate a transition toward an ohmic behavior upon electrochemical oxidation, illustrating the change in the conduction mode going from a semiconducting to a conducting state (Figure 5b). The nonself-assembling control triarylamine was also oxidized by performing $I-V$ sweeps up to 2 V, yet no change to the $I-V$ curve shape was observed. In addition, it was possible to form the nanowires directly inside the device by first inserting a solution of nonassembled TATA **1** (5:3 methanol:toluene with 5% tetrachloroethane) and by subsequent light irradiation. The 4 orders of magnitude increase of the conductivity and the characteristic linear $I-V$ curve remained after the light was turned off (Figure 5c), demonstrating a self-construction process in a gap as large as 4 μm between simple commercially available ITO plates.[23]

We finally probed the conductivity improvement afforded by the light-induced healing process in the fibers. After irradiation of the initial gel of TATA **1** with a short pulse of light (15 s with the voltage held at 0.1 V), an increase of the conductivity was measured afterward in the dark, with a gain comprised between 30 and 50% (Figure 5d and Figure S19). This value can be correlated with an increase of the coherence length and a decrease of structural defects in the polymer, as determined by SAXS and AFM (see above). We also measured a delay time (T_d) between switching the light off and reaching the maximum conductivity value, and interestingly an inverse dependence of T_d on the applied voltage was noticed (inset in Figure 5d). We postulate that this further increase reflects the supramolecular optimization of the fibers thanks to the increased photoinduced

dx.doi.org/10.1021/ja5044006 | J. Am. Chem. Soc. 2014, 136, 11382−11388

charge injection linked to the polarons' diffusion in the electric field.

CONCLUSIONS

In conclusion, we have described the synthesis and the unique properties of a new class of soft supramolecular polymers made of columnar stacks of tris-amide triarylamines. These one-dimensional fibers can be oxidized to their radical cation by light (photodoping) or electrochemically. The resulting presence of delocalized Pauli spins and polaronic absorption band shows that this supramolecular system has similar charge-transport characteristics to those observed in metallic conducting conjugated polymers. This first demonstration that supramolecular polymers can present electronic, magnetic, and optical signatures similar to those measured through-bond in the best conjugated polymers extends the current understanding of both fields and unifies them. In addition, we have shown that the induced through-space mixed-valence charge transfer within their structure behave as "supramolecular polarons" which diffuse along the fibers and fix structural defects of the stacked structure, representing a novel cooperative healing mechanism thanks to the presence of the charge carrier itself. The capacity of soft supramolecular self-assemblies to self-optimize their conduction properties[44−46] provides alternatives to conventional organic metals in terms of responsiveness, healing, and processability, which is of interest for applications in organic electronics and spintronics.

ASSOCIATED CONTENT

Supporting Information

Synthetic protocols and characterization of TATA **1**−**3**, organogelation properties, supplementary AFM characterizations, X-ray scattering data, DFT calculations, local and extended charge transfer analyses, and additional conductivity characterizations. This material is available free of charge via the Internet at http://pubs.acs.org.

AUTHOR INFORMATION

Corresponding Author

giuseppone@unistra.fr

Notes

The authors declare no competing financial interests.

ACKNOWLEDGMENTS

The research leading to these results has received funding from the European Research Council under the European Community's Seventh Framework Program (FP7/2007-2013)/ERC Starting Grant Agreement No. 257099 (N.G.). We wish to thank the Centre National de la Recherche Scientifique (CNRS), the COST action (CM 1304), the international center for Frontier Research in Chemistry (icFRC), the Laboratory of Excellence for Complex System Chemistry (LabEx CSC), the University of Strasbourg (UdS), and the Institut Universitaire de France (IUF). We are grateful to ANR (Agence Nationale de la Recherche) for financial support (projects STANWs and Multiself). We thank Prof. T. W. Ebbesen for fruitful discussions on this work. We thank Dr. Marc Schmutz for FFEM replicas preparation.

REFERENCES

(1) Forrest, S. R. *Nature* **2004**, *428*, 911−918.
(2) Miller, R. D.; Chandross, E. A. *Chem. Rev.* **2010**, *110*, 1−2.
(3) Shirakawa, H.; Louis, E. J.; MacDiarmid, A. G.; Chiang, C. K.; Heeger, A. J. *J. Chem. Soc. Chem. Commun.* **1977**, 578−580.
(4) Heeger, A. J. *Rev. Mod. Phys.* **2001**, *73*, 681−700.
(5) Koezuka, H.; Tsumura, A.; Ando, T. *Synth. Met.* **1987**, *18*, 699−704.
(6) Burroughes, J. H.; Bradley, D. D. C.; Brown, A. R.; Marks, R. N.; Mackay, K.; Friend, R. H.; Burns, P. L.; Holmes, A. B. *Nature* **1990**, *347*, 539−541.
(7) Sariciftci, N. S.; Smilowitz, L.; Heeger, A. J.; Wudl, F. *Science* **1992**, *258*, 1474−1476.
(8) MacDiarmid, A. G. *Angew. Chem., Int. Ed.* **2001**, *40*, 2581−2590.
(9) Fabretto, M. V.; Evans, D. R.; Mueller, M.; Zuber, K.; Hojati-Talemi, P.; Short, R. D.; Wallace, G. G.; Murphy, P. J. *Chem. Mater.* **2012**, *24*, 3998−4003.
(10) Xia, Y.; Sun, K.; Ouyang, J. *Adv. Mater.* **2012**, *24*, 2436−2440.
(11) Singh, M.; Haverinen, H. M.; Dhagat, P.; Jabbour, G. E. *Adv. Mater.* **2010**, *22*, 673−685.
(12) Sirringhaus, H.; Kawase, T.; Friend, R. H.; Shimoda, T.; Inbasekaran, M.; Wu, W.; Woo, E. P. *Science* **2000**, *290*, 2123−2126.
(13) Bubnova, O.; Khan, Z. U.; Wang, H.; Braun, S.; Evans, D. R.; Fabretto, M.; Hojati-Talemi, P.; Dagnelund, D.; Arlin, J.-B.; Geerts, Y. H.; Desbief, S.; Breiby, D. W.; Andreasen, J. W.; Lazzaroni, R.; Chen, W. M.; Zozoulenko, I.; Fahlman, M.; Murphy, P. J.; Berggren, M.; Crispin, X. *Nat. Mater.* **2014**, *13*, 190−194.
(14) Bubnova, O.; Khan, Z. U.; Malti, A.; Braun, S.; Fahlman, M.; Berggren, M.; Crispin, X. *Nat. Mater.* **2011**, *10*, 429−433.
(15) Lin, W.-P.; Liu, S.-J.; Gong, T.; Zhao, Q.; Huang, W. *Adv. Mater.* **2014**, *26*, 570−606.
(16) Bredas, J.-L.; Street, G. B. *Acc. Chem. Res.* **1985**, *18*, 309−315.
(17) Kaiser, A. B. *Adv. Mater.* **2001**, *13*, 927−941.
(18) Hoffmann, S. T.; Jaiser, F.; Hayer, A.; Bässler, H.; Unger, T.; Athanasopoulos, S.; Neher, D.; Köhler, A. *J. Am. Chem. Soc.* **2013**, *135*, 1772−1782.
(19) Kohlman, R. S.; Zibold, A.; Tanner, D. B.; Ihas, G. G.; Ishiguro, T.; Min, Y. G.; MacDiarmid, A. G.; Epstein, A. J. *Phys. Rev. Lett.* **1997**, *78*, 3915−3918.
(20) Lee, K.; Cho, S.; Heum Park, S.; Heeger, A. J.; Lee, C.-W.; Lee, S.-H. *Nature* **2006**, *441*, 65−68.
(21) Cohen, M. J.; Coleman, L. B.; Garito, A. F.; Heeger, A. J. *Phys. Rev. B* **1974**, *10*, 1298−1307.
(22) Moulin, E.; Niess, F.; Maaloum, M.; Buhler, E.; Nyrkova, I.; Giuseppone, N. *Angew. Chem., Int. Ed.* **2010**, *49*, 6974−6978.
(23) Faramarzi, V.; Niess, F.; Moulin, E.; Maaloum, M.; Dayen, J.-F.; Beaufrand, J.-B.; Zanettini, S.; Doudin, B.; Giuseppone, N. *Nat. Chem.* **2012**, *4*, 485−490.
(24) Aida, T.; Meijer, E. W.; Stupp, S. I. *Science* **2012**, *335*, 813−817.
(25) Cordier, P.; Tournilhac, F.; Soulie-Ziakovic, C.; Leibler, L. *Nature* **2008**, *451*, 977−980.
(26) Yang, Y.; Urban, M. W. *Chem. Soc. Rev.* **2013**, *42*, 7446−7467.
(27) Non-hydrogen-bonded amides have N-H stretching frequency between 3400 and 3500 cm^{-1} as opposed to 3350−3100 cm^{-1} for hydrogen bonded amides. Likewise the C═O stretch shifts from around 1685 to 1650 cm^{-1} upon hydrogen bonding. The IR frequency shifts we report for both functional groups correspond to the presence of hydrogen bonded amides. See: Pretsch, E. Bühlmann, P.; Badertscher, M. *Structure Determination of Organic Compounds*, 4th ed.; Springer: New York, 2009.
(28) Zhao, Y.; Truhlar, D. G. *Acc. Chem. Res.* **2008**, *41*, 157−167.
(29) Zhao, Y.; Truhlar, D. *Theor. Chem. Acc.* **2008**, *120*, 215−241.
(30) Steinmann, S. N.; Piemontesi, C.; Delachat, A.; Corminboeuf, C. *J. Chem. Theory Comput.* **2012**, *8*, 1629−1640.
(31) Heckmann, A.; Lambert, C. *Angew. Chem., Int. Ed.* **2012**, *51*, 326−392.
(32) Robin, M. B.; Day, P. Mixed valence chemistry - A survey and classification. In *Advances in Inorganic Chemistry and Radiochemistry*; Emeléus, H. J., Sharpe, A. G., Eds.; Academic Press Inc.: New York, 1968; Vol. *10*, pp 274−422.

(33) Lancaster, K.; Odom, S. A.; Jones, S.; Thayumanavan, S.; Marder, S. R.; Bredas, J.-L.; Coropceanu, V.; Barlow, S. *J. Am. Chem. Soc.* **2009**, *131*, 1717−1723.
(34) Rivnay, J.; Mannsfeld, S. C. B.; Miller, C. E.; Salleo, A.; Toney, M. F. *Chem. Rev.* **2012**, *112*, 5488−5519.
(35) Marcus, R. A. *Angew. Chem., Int. Ed.* **1993**, *32*, 1111−1121.
(36) Hush, N. S. *Electrochim. Acta* **1968**, *13*, 1005−1023.
(37) Scheblykin, I. G.; Yartsev, A.; Pullerits, T.; Gulbinas, V.; Sundström, V. *J. Phys. Chem. B* **2007**, *111*, 6303−6321.
(38) Lin, H.; Tabaei, S. R.; Thomsson, D.; Mirzov, O.; Larsson, P.-O.; Scheblykin, I. G. *J. Am. Chem. Soc.* **2008**, *130*, 7042−7051.
(39) Krinichnyi, V. I.; Konkin, A. L.; Monkman, A. P. *Synth. Met.* **2012**, *162*, 1147−1155.
(40) Bleaney, B.; Bowers, K. D. *Proc. R. Soc. London, A* **1952**, *214*, 451−465.
(41) Eaton, S. S.; More, K. M.; Sawant, B. M.; Eaton, G. R. *J. Am. Chem. Soc.* **1983**, *105*, 6560−6567.
(42) Lee, K.; Heeger, A. J. *Synth. Met.* **1997**, *84*, 715−718.
(43) Beljonne, D.; Cornil, J.; Sirringhaus, H.; Brown, P. J.; Shkunov, M.; Friend, R. H.; Brédas, J.-L. *Adv. Funct. Mater.* **2001**, *11*, 229−234.
(44) Busseron, E.; Ruff, Y.; Moulin, E.; Giuseppone, N. *Nanoscale* **2013**, *5*, 7098−7140.
(45) Giuseppone, N. *Acc. Chem. Res.* **2012**, *45*, 2178−2188.
(46) Moulin, E.; Cid, J.-J.; Giuseppone, N. *Adv. Mat.* **2013**, *25*, 477−487.